

Dalitz Analysis of Three-body Charmless $B^0 \rightarrow K^0 \pi^+ \pi^-$ Decay

A. Garmash,³⁵ K. Abe,⁸ I. Adachi,⁸ H. Aihara,⁴⁶ D. Anipko,¹ K. Arinstein,¹ V. Aulchenko,¹ T. Aushev,^{18,13} S. Bahinipati,⁴ A. M. Bakich,⁴¹ V. Balagura,¹³ E. Barberio,²¹ M. Barbero,⁷ A. Bay,¹⁸ I. Bedny,¹ K. Belous,¹² U. Bitenc,¹⁴ I. Bizjak,¹⁴ S. Blyth,²⁴ A. Bondar,¹ A. Bozek,²⁷ M. Bračko,^{8,20,14} T. E. Browder,⁷ M.-C. Chang,⁵ Y. Chao,²⁶ A. Chen,²⁴ K.-F. Chen,²⁶ W. T. Chen,²⁴ B. G. Cheon,³ R. Chistov,¹³ Y. Choi,⁴⁰ Y. K. Choi,⁴⁰ S. Cole,⁴¹ J. Dalseno,²¹ M. Dash,⁵⁰ J. Dragic,⁸ A. Drutskoy,⁴ S. Eidelman,¹ D. Epifanov,¹ N. Gabyshev,¹ T. Gershon,⁸ A. Go,²⁴ G. Gokhroo,⁴² B. Golob,^{19,14} H. Ha,¹⁶ J. Haba,⁸ K. Hayasaka,²² H. Hayashii,²³ M. Hazumi,⁸ D. Heffernan,³² T. Hokuue,²² Y. Hoshi,⁴⁴ S. Hou,²⁴ W.-S. Hou,²⁶ Y. B. Hsiung,²⁶ T. Iijima,²² K. Ikado,²² A. Imoto,²³ K. Inami,²² A. Ishikawa,⁴⁶ H. Ishino,⁴⁷ R. Itoh,⁸ M. Iwasaki,⁴⁶ Y. Iwasaki,⁸ J. H. Kang,⁵¹ P. Kapusta,²⁷ H. Kawai,² T. Kawasaki,²⁹ H. Kichimi,⁸ H. J. Kim,¹⁷ Y. J. Kim,⁶ K. Kinoshita,⁴ P. Križan,^{19,14} P. Krokovny,⁸ R. Kulasiri,⁴ R. Kumar,³³ C. C. Kuo,²⁴ A. Kuzmin,¹ Y.-J. Kwon,⁵¹ S. E. Lee,³⁸ T. Lesiak,²⁷ J. Li,⁷ S.-W. Lin,²⁶ Y. Liu,⁶ G. Majumder,⁴² F. Mandl,¹¹ T. Matsumoto,⁴⁸ S. McOnie,⁴¹ W. Mitaroff,¹¹ K. Miyabayashi,²³ H. Miyake,³² H. Miyata,²⁹ Y. Miyazaki,²² R. Mizuk,¹³ D. Mohapatra,⁵⁰ G. R. Moloney,²¹ Y. Nagasaka,⁹ E. Nakano,³¹ M. Nakao,⁸ Z. Natkaniec,²⁷ S. Nishida,⁸ O. Nitoh,⁴⁹ S. Noguchi,²³ T. Ohshima,²² S. Okuno,¹⁵ S. L. Olsen,⁷ Y. Onuki,³⁶ P. Pakhlov,¹³ G. Pakhlova,¹³ H. Park,¹⁷ L. S. Peak,⁴¹ R. Pestotnik,¹⁴ L. E. Pilonen,⁵⁰ A. Poluektov,¹ H. Sahoo,⁷ Y. Sakai,⁸ N. Satoyama,³⁹ T. Schietinger,¹⁸ O. Schneider,¹⁸ J. Schümamm,²⁵ C. Schwanda,¹¹ A. J. Schwartz,⁴ K. Senyo,²² M. Shapkin,¹² H. Shibuya,⁴³ B. Shwartz,¹ V. Sidorov,¹ A. Sokolov,¹² A. Somov,⁴ S. Stanič,³⁰ M. Starič,¹⁴ H. Stoeck,⁴¹ K. Sumisawa,⁸ T. Sumiyoshi,⁴⁸ S. Y. Suzuki,⁸ F. Takasaki,⁸ K. Tamai,⁸ M. Tanaka,⁸ G. N. Taylor,²¹ Y. Teramoto,³¹ X. C. Tian,³⁴ K. Trabelsi,⁷ T. Tsukamoto,⁸ S. Uehara,⁸ T. Uglov,¹³ K. Ueno,²⁶ Y. Unno,³ S. Uno,⁸ P. Urquijo,²¹ Y. Ushiroda,⁸ Y. Usov,¹ G. Varner,⁷ K. E. Varvell,⁴¹ S. Villa,¹⁸ C. H. Wang,²⁵ M.-Z. Wang,²⁶ Y. Watanabe,⁴⁷ E. Won,¹⁶ C.-H. Wu,²⁶ Q. L. Xie,¹⁰ B. D. Yabsley,⁴¹ A. Yamaguchi,⁴⁵ Y. Yamashita,²⁸ M. Yamauchi,⁸ C. C. Zhang,¹⁰ L. M. Zhang,³⁷ Z. P. Zhang,³⁷ V. Zhilich,¹ and A. Zupanc¹⁴

(The Belle Collaboration)

¹*Budker Institute of Nuclear Physics, Novosibirsk*

²*Chiba University, Chiba*

³*Chonnam National University, Kwangju*

⁴*University of Cincinnati, Cincinnati, Ohio 45221*

⁵*Department of Physics, Fu Jen Catholic University, Taipei*

⁶*The Graduate University for Advanced Studies, Hayama, Japan*

⁷*University of Hawaii, Honolulu, Hawaii 96822*

⁸*High Energy Accelerator Research Organization (KEK), Tsukuba*

⁹*Hiroshima Institute of Technology, Hiroshima*

¹⁰*Institute of High Energy Physics, Chinese Academy of Sciences, Beijing*

¹¹*Institute of High Energy Physics, Vienna*

¹²*Institute of High Energy Physics, Protvino*

¹³*Institute for Theoretical and Experimental Physics, Moscow*

¹⁴*J. Stefan Institute, Ljubljana*

¹⁵*Kanagawa University, Yokohama*

¹⁶*Korea University, Seoul*

¹⁷*Kyungpook National University, Taegu*

¹⁸*Swiss Federal Institute of Technology of Lausanne, EPFL, Lausanne*

¹⁹*University of Ljubljana, Ljubljana*

²⁰*University of Maribor, Maribor*

²¹*University of Melbourne, Victoria*

²²*Nagoya University, Nagoya*

²³*Nara Women's University, Nara*

²⁴*National Central University, Chung-li*

²⁵*National United University, Miao Li*

²⁶*Department of Physics, National Taiwan University, Taipei*

²⁷*H. Niewodniczanski Institute of Nuclear Physics, Krakow*

²⁸*Nippon Dental University, Niigata*

²⁹*Niigata University, Niigata*

³⁰*University of Nova Gorica, Nova Gorica*

³¹*Osaka City University, Osaka*

³²*Osaka University, Osaka*

³³*Panjab University, Chandigarh*

³⁴*Peking University, Beijing*

³⁵*Princeton University, Princeton, New Jersey 08544*

³⁶RIKEN BNL Research Center, Upton, New York 11973

³⁷University of Science and Technology of China, Hefei

³⁸Seoul National University, Seoul

³⁹Shinshu University, Nagano

⁴⁰Sungkyunkwan University, Suwon

⁴¹University of Sydney, Sydney NSW

⁴²Tata Institute of Fundamental Research, Bombay

⁴³Toho University, Funabashi

⁴⁴Tohoku Gakuin University, Tagajo

⁴⁵Tohoku University, Sendai

⁴⁶Department of Physics, University of Tokyo, Tokyo

⁴⁷Tokyo Institute of Technology, Tokyo

⁴⁸Tokyo Metropolitan University, Tokyo

⁴⁹Tokyo University of Agriculture and Technology, Tokyo

⁵⁰Virginia Polytechnic Institute and State University, Blacksburg, Virginia 24061

⁵¹Yonsei University, Seoul

We report results of a Dalitz plot analysis of the three-body charmless $B^0 \rightarrow K^0\pi^+\pi^-$ decay. The analysis is performed with a data sample that contains 388 million $B\bar{B}$ pairs collected near the $\Upsilon(4S)$ resonance with the Belle detector at the KEKB asymmetric energy e^+e^- collider. Measurements of branching fractions for the quasi-two-body decays $B^0 \rightarrow \rho(770)^0 K^0$, $B^0 \rightarrow f_0(980)K^0$, $B^0 \rightarrow K^*(892)^+\pi^-$, $B^0 \rightarrow K^*(1430)^+\pi^-$, and upper limits on several other quasi-two-body decay modes are reported.

PACS numbers: 13.20.He, 13.25.Hw, 13.30.Eg, 14.40.Nd

I. INTRODUCTION

Decays of B mesons to three-body charmless hadronic final states have attracted considerable attention in recent years. An amplitude analysis for a number of three-body final states has been performed (for example, $K^+K^+K^-$, $K^+\pi^+\pi^-$, $K^+\pi^-\pi^0$), where branching fractions for many quasi-two-body intermediate states have been measured for the first time or with a significantly improved accuracy.

In addition to providing a rich laboratory for studying B meson decay dynamics, three-body charmless final states open new possibilities for CP violation studies. Several new ideas utilizing three-body final states have been proposed [1]. Experimentally, studies of CP violation have been done with most of the final states mentioned above, yielding some interesting results. For example, the first evidence for direct CP violation in charged B meson decays to the $\rho(770)^0 K^\pm$ final states has been recently found through the amplitude analysis of the three-body $B^\pm \rightarrow K^\pm\pi^\pm\pi^\mp$ decay [2]. Time-dependent CP violation was measured in $B^0 \rightarrow K^+K^-K^0$ [3, 4] and $B^0 \rightarrow K_S^0 K_S^0 K_S^0$ [5, 6] three-body decays, which occur dominantly via the $b \rightarrow s$ penguin transition. Measurements of $\sin 2\phi_1$ in $b \rightarrow s$ penguin-dominated decays provide an important test of the Standard Model. The quasi-two-body $B^0 \rightarrow f_0(980)K_S^0$ channel that contributes to the three-body $K_S^0\pi^+\pi^-$ final state is also expected to be dominated by the $b \rightarrow s$ penguin transition and thus has been used for the measurement of $\sin 2\phi_1$ [3, 7, 8]. However, since the $f_0(980)$ has a significant natural width, nearby resonant states (for example the $\rho(770)^0$ is particularly important as the combined CP parity of the $B^0 \rightarrow \rho(770)K_S^0$ is opposite

to that of the $B^0 \rightarrow f_0(980)K_S^0$) might contribute to the $f_0(980)$ mass region and an accurate estimation of these contributions is required for a correct interpretation of the results. This can only be done via an amplitude (Dalitz) analysis of the three-body $B^0 \rightarrow K^0\pi^+\pi^-$ decay.

In this paper we report first results of a Dalitz plot analysis of the three-body charmless $B^0 \rightarrow K^0\pi^+\pi^-$ decay. The analysis is based on a 357 fb^{-1} data sample containing $388 \times 10^{-6} B\bar{B}$ pairs, collected with the Belle detector operating at the KEKB asymmetric-energy e^+e^- collider [9] with a center-of-mass (c.m.) energy at the $\Upsilon(4S)$ resonance. For the study of the $e^+e^- \rightarrow q\bar{q}$ continuum background, we use a data sample (that amounts to about 10% of the on-resonance sample) taken 60 MeV below the $\Upsilon(4S)$ resonance.

II. THE BELLE DETECTOR

The Belle detector [10] is a large-solid-angle magnetic spectrometer based on a 1.5 T superconducting solenoid magnet. Charged particle tracking is provided by a silicon vertex detector and a 50-layer central drift chamber (CDC) that surround the interaction point. Charged hadron identification is provided by dE/dx measurements in the CDC, an array of 1188 aerogel Čerenkov counters (ACC), and a barrel-like array of 128 time-of-flight scintillation counters (TOF); information from the three subdetectors is combined to form a single likelihood ratio for each pair of hadron species that is then used for pion, kaon and proton discrimination. Electromagnetic showering particles are detected in an array of 8736 CsI(Tl) crystals (ECL) that covers the same solid

angle as the charged particle tracking system. Electron identification is based on a combination of dE/dx measurements in the CDC, the response of the ACC, and the position, shape and total energy deposition of the shower detected in the ECL. The electron identification efficiency is greater than 92% for tracks with $p_{\text{lab}} > 1.0$ GeV/ c and the hadron misidentification probability is below 0.3%. The magnetic field is returned via an iron yoke that is instrumented to detect muons and K_L^0 mesons. We use a GEANT-based Monte Carlo (MC) simulation to model the response of the detector and determine its acceptance [11].

III. EVENT RECONSTRUCTION

Candidate charged pions from B meson decay are required to be consistent with having originated from the interaction point and to have momenta transverse to the beam greater than 0.1 GeV/ c . To reduce the combinatorial background, we impose a requirement on the particle identification variable that has 93% efficiency and about 15% fake rate from misidentified kaons. Tracks that are positively identified as electrons or protons are excluded. We fit these candidate pions to the common vertex to determine the B meson decay vertex. Neutral kaons are reconstructed via the decay $K^0 \rightarrow \pi^+\pi^-$. The invariant mass of the two oppositely charged tracks is required to be within 12 MeV/ c^2 of the nominal K_S^0 mass. The direction of flight of the K_S^0 candidate is required to be consistent with the direction of its vertex displacement with respect to the B decay vertex.

B candidates are identified using two kinematic variables: the beam-constrained mass $M_{\text{bc}} = \frac{1}{c^2} \sqrt{E_{\text{beam}}^{*2} - c^2 |\sum_i \mathbf{p}_i|^2}$, and the energy difference $\Delta E = (\sum_i \sqrt{c^2 |\mathbf{p}_i|^2 + c^4 m_i^2}) - E_{\text{beam}}^*$, where the summation is over all particles from a B candidate; \mathbf{p}_i and m_i are their c.m. three-momenta and masses, respectively; E_{beam}^* is the beam energy in the c.m. frame. The signal M_{bc} resolution is mainly determined by the beam energy spread and amounts to 2.9 MeV/ c^2 . The signal ΔE shape is fit to a sum of two Gaussian functions (core and tail) with a common mean.

The dominant background is due to $e^+e^- \rightarrow q\bar{q}$ ($q = u, d, s$ and c quarks) continuum events. We suppress this background using variables that characterize the event topology. Since the two B mesons produced from an $\Upsilon(4S)$ decay are nearly at rest in the c.m. frame, their decay products are uncorrelated and the event tends to be spherical. In contrast, hadrons from continuum $q\bar{q}$ events tend to exhibit a two-jet structure. We use θ_{thr} , which is the angle between the thrust axis of the B candidate and that of the rest of the event, to discriminate between the two cases. The distribution of $|\cos \theta_{\text{thr}}|$ is strongly peaked near $|\cos \theta_{\text{thr}}| = 1.0$ for $q\bar{q}$ events and is nearly flat for $B\bar{B}$ events. We require $|\cos \theta_{\text{thr}}| < 0.80$ eliminating about 83% of the continuum background while retaining 79% of the signal events.

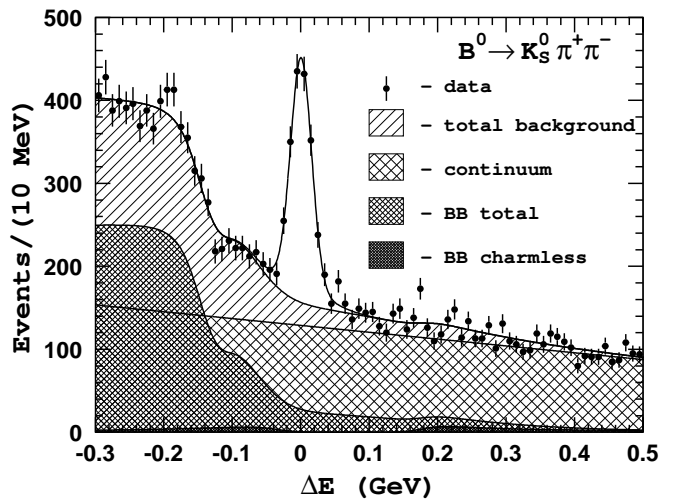


FIG. 1: ΔE distribution for the $B^0 \rightarrow K_S^0 \pi^+ \pi^-$ candidate events with $|M_{\text{bc}} - M_B| < 7.5$ MeV/ c^2 . Points with error bars are data; the upper curve is the fit result; the hatched histograms are various background components.

For further suppression of the continuum background, we use a Fisher discriminant formed from 11 variables: nine variables that characterize the angular distribution of the momentum flow in the event with respect to the B candidate thrust axis, the angle of the B candidate thrust axis with respect to the beam axis, and the angle between the B candidate momentum and the beam axis. Use of such a Fisher discriminant rejects about 89% of the remaining continuum background with 53% efficiency for the signal. A more detailed description of the background suppression technique can be found in Ref. [12] and references therein.

From MC study we find that the backgrounds originating from other B meson decays that peak in the signal region are due to $B^0 \rightarrow D^- [K_S^0 \pi^-] \pi^+$ as well as $B^0 \rightarrow J/\psi [\mu^+ \mu^-] K_S^0$ and $B^0 \rightarrow \psi(2S) [\mu^+ \mu^-] K_S^0$ decays with muons misidentified as pions. We veto these backgrounds by requiring $|M(K_S^0 \pi^-) - M_D| > 100$ MeV/ c^2 , $|M(\pi^+ \pi^-)_{\mu\mu} - M_{J/\psi}| > 70$ MeV/ c^2 and $|M(\pi^+ \pi^-)_{\mu\mu} - M_{\psi(2S)}| > 50$ MeV/ c^2 , with a muon mass assignment used here for the pion candidates. To suppress the background due to K/π misidentification, we exclude candidates that are consistent with the $D^- \rightarrow K_S^0 K^-$ hypothesis within 15 MeV/ c^2 ($\sim 2.5\sigma$), regardless of the particle identification information. There is also a large background from the $B \rightarrow D[K\pi\pi]\pi$ channel and from the $B \rightarrow D^{(*)}\pi$ channel with a subsequent semileptonic $D \rightarrow K\mu\nu_\mu$ decay. However, these modes do not peak in the signal region and contribute mainly to the $\Delta E < 0$ region. The most significant backgrounds from charmless B decays originate from $B^0 \rightarrow \eta'[\pi^+\pi^-\gamma]K_S^0$ and $B^\pm \rightarrow K_S^0 \pi^\pm$ decays. In the latter case an additional soft pion is randomly picked up to form a $K_S^0 \pi^+ \pi^-$ combination. We determine the ΔE shape for these backgrounds from MC simulation and take them into account when

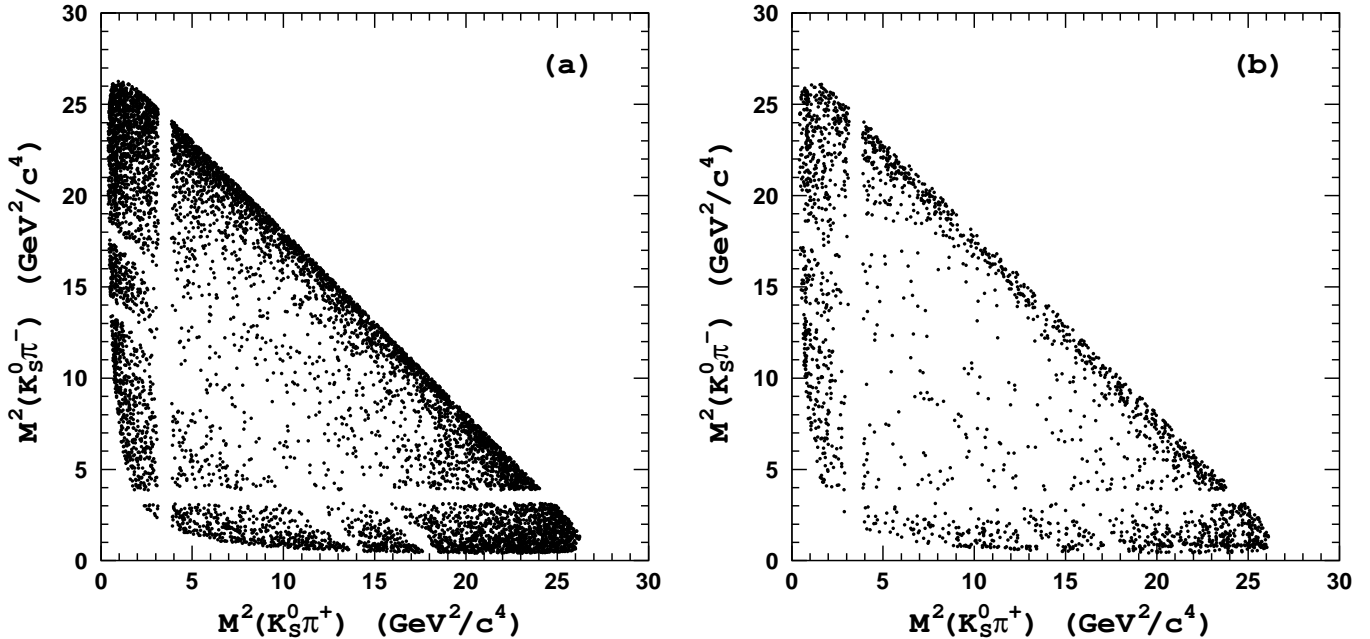


FIG. 2: Dalitz plots for events in the (a) $M_{bc}-\Delta E$ sidebands and in the (b) B signal region.

fitting the data.

The ΔE distribution for $K_S^0\pi^+\pi^-$ combinations that pass all the selection requirements is shown in Fig. 1, where a clear peak in the signal region is observed. In the fit to the ΔE distribution we fix the shape of the $B\bar{B}$ background component from MC and let the normalization float. The shape of the $q\bar{q}$ background is parametrized by a linear function with slope and normalization as free fit parameters. For the signal component the width (σ) and the relative fraction of the tail Gaussian function are fixed at 30 MeV and 0.19, respectively, as determined from signal MC simulation. The common mean of the two Gaussian functions and the width of the core Gaussian are allowed to float and found to be 0.7 ± 0.6 MeV and 15.3 ± 0.9 MeV, respectively. The fit yields 1229 ± 62 signal $B^0 \rightarrow K_S^0\pi^+\pi^-$ events.

IV. AMPLITUDE ANALYSIS

The amplitude analysis of the three-body $B^0 \rightarrow K^0\pi^+\pi^-$ signal is performed by means of an unbinned maximum likelihood fit. In general, we follow the procedure we used for the analysis of the decay $B^+ \rightarrow K^+\pi^+\pi^-$ described in detail in Ref. [13]. For the analysis we select events in the B signal region defined as an ellipse around the M_{bc} and ΔE signal mean values:

$$\left[\frac{M_{bc} - M_B}{7.5 \text{ MeV}/c^2} \right]^2 + \left[\frac{\Delta E}{40 \text{ MeV}} \right]^2 < 1.$$

To determine the distribution of background events over the phase space (Dalitz plot) we use events in the $M_{bc} -$

ΔE sidebands defined as

$$0.05 \text{ GeV}/c^2 < |M(K\pi\pi) - M_B| < 0.10 \text{ GeV}/c^2; \\ P(K\pi\pi) < 0.48 \text{ GeV}/c$$

and

$$|M(K\pi\pi) - M_B| < 0.10 \text{ GeV}/c^2; \\ 0.48 \text{ GeV}/c < P(K\pi\pi) < 0.65 \text{ GeV}/c,$$

where $M(K\pi\pi)$ and $P(K\pi\pi)$ are the three-particle invariant mass and three-particle momentum in the c.m. frame. The total number of events in the signal (sideband) region is 2207 (8159). The relative fraction of signal events in the signal region is 0.521 ± 0.025 .

A. Fit to Sideband Events

The Dalitz plot for events in the $M_{bc} - \Delta E$ sideband region is shown in Fig. 2(a) where visible gaps are due to vetoes applied on invariant masses of two-particle combinations. We use the following empirical parametrization to describe the distribution of background events over the Dalitz plot:

$$B(K_S^0\pi^\pm\pi^\mp) = \alpha_1(e^{-\beta_1 s_{12}} + e^{-\beta_1 s_{13}}) + \alpha_2 e^{-\beta_2 s_{23}} \\ + \alpha_3(e^{-\beta_3 s_{12} - \beta_4 s_{23}} + e^{-\beta_3 s_{13} - \beta_4 s_{23}}) \\ + \alpha_4 e^{-\beta_5 (s_{12} + s_{13})} \\ + \gamma_1 (|BW_1(K^*(892)^-)|^2 + |BW_1(K^*(892)^+)|^2) \\ + \gamma_2 |BW(\rho(770)^0)|^2, \quad (1)$$

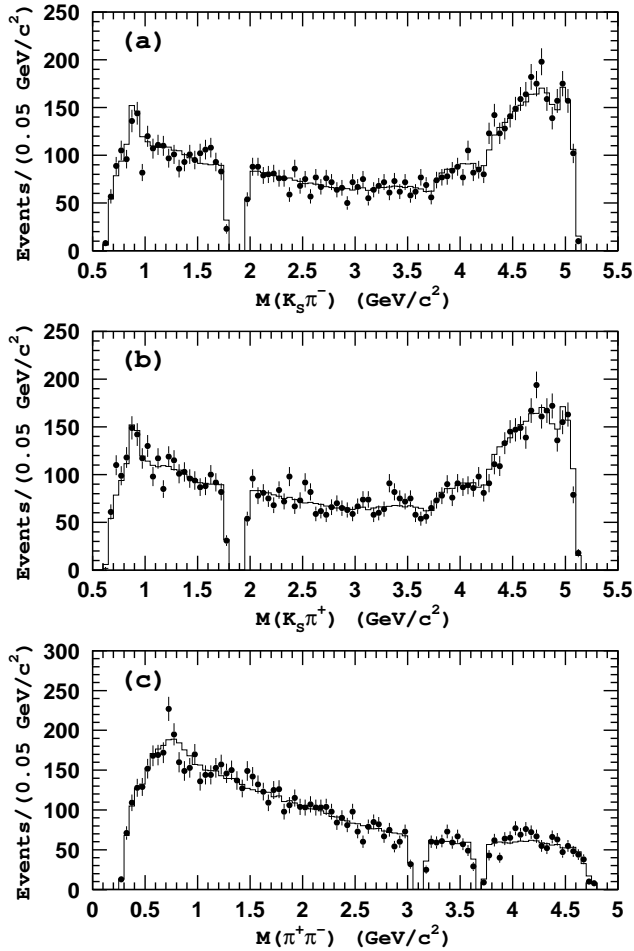


FIG. 3: Results of the best fit to events in the $\Delta E - M_{bc}$ sidebands. Points with error bars are data; histograms are fit results.

where $s_{12} \equiv M^2(K_S^0 \pi^-)$, $s_{13} \equiv M^2(K_S^0 \pi^+)$, $s_{23} \equiv M^2(\pi^+ \pi^-)$ and α_i ($\alpha_1 \equiv 1.0$), β_i and γ_i are fit parameters; BW is a Breit-Wigner function. The first two terms in Eq. (1) are introduced to describe the excess of background events in the two-particle low invariant mass regions (borders of the Dalitz plot). This enhancement originates mainly from $e^+ e^- \rightarrow q\bar{q}$ continuum events; due to the jet-like structure of this background, all three particles in a three-body combination have almost collinear momenta. Hence, the invariant mass of at least one pair of particles is in the low mass region. In addition, it is often the case that two high momentum particles are combined with a low momentum particle to form a B candidate. In this case there are two pairs with low invariant masses and one pair with high invariant mass, resulting in even stronger enhancement of the background in the corners of the Dalitz plot. This is taken into account by terms proportional to α_3 and α_4 in Eq. (1). To account for a possible contribution from real $K^*(892)^\pm$ and $\rho(770)^0$ mesons, we introduce two more terms in Eq. (1), that are (non-interfering) squared Breit-Wigner ampli-

tudes, with masses and widths fixed at world average values [14]. The two-particle invariant mass projections for the sideband data and the fit results are shown in Fig. 3.

B. Fit to Signal Events

The Dalitz plot for events in the signal region is shown in Fig. 2(b); Figure 4 shows the two-particle invariant mass distributions. In an attempt to describe all the features of the $K_S^0 \pi^\pm$ and $\pi^+ \pi^-$ mass spectra visible in Fig. 4, we use a matrix element similar to that constructed in the analysis of the $B^+ \rightarrow K^+ \pi^+ \pi^-$ decay [13]:

$$\begin{aligned}
 \mathcal{M}(K^0 \pi^+ \pi^-) = & a_{K^*} e^{i\delta_{K^*}} \mathcal{A}_1(\pi^+ K^0 \pi^- | K^*(892)^+) \\
 & + a_{K_0^*} e^{i\delta_{K_0^*}} \mathcal{A}_0(\pi^+ K^0 \pi^- | K_0^*(1430)^+) \\
 & + a_\rho e^{i\delta_\rho} \mathcal{A}_1(K^0 \pi^+ \pi^- | \rho(770)^0) \\
 & + a_{f_0} e^{i\delta_{f_0}} \mathcal{A}_{\text{Flatte}}(K^0 \pi^+ \pi^- | f_0(980)) \\
 & + a_{f_X} e^{i\delta_{f_X}} \mathcal{A}_0(K^0 \pi^+ \pi^- | f_X(1300)) \\
 & + a_{\chi_{c0}} e^{i\delta_{\chi_{c0}}} \mathcal{A}_0(K^0 \pi^+ \pi^- | \chi_{c0}) \\
 & + \mathcal{A}_{\text{nr}}(K^0 \pi^+ \pi^-), \tag{2}
 \end{aligned}$$

where relative amplitudes a_i and phases δ_i are fit parameters. Each quasi-two-body amplitude \mathcal{A}_J is parametrized as

$$\mathcal{A}_J = F_B F_R^{(J)} BW_J T_J, \tag{3}$$

where J is the spin of an intermediate resonant state; BW_J is the Breit-Wigner function; F_B is the B meson decay form factor parametrized in a single-pole approximation [15]; $F_R^{(J)}$ is the Blatt-Weisskopf form factor [16] for the intermediate resonance decay; and T_J is the function that describes angular correlations between final state particles. For more details, see Ref. [13]. The $f_0(980)$ lineshape is parametrized with a Flatté function [17] with parameters fixed at the values determined in the analysis of the $B^+ \rightarrow K^+ \pi^+ \pi^-$ decay [2]: $M = 0.950 \pm 0.009(\text{stat.})$ GeV/ c^2 and coupling constants $g_{\pi\pi} = 0.23 \pm 0.05(\text{stat.})$ and $g_{KK} = 0.73 \pm 0.30(\text{stat.})$ [18]. An additional amplitude $f_X(1300)$ is introduced to account for an excess of signal events observed at $M(\pi^+ \pi^-) \simeq 1.3$ GeV/ c^2 . As found in Ref. [13], if approximated by a single resonant state, it is best described by a scalar amplitude. We fix the mass and width of the $f_X(1300)$ at values determined in Ref. [2]: $M = 1.449 \pm 0.013(\text{stat.})$ GeV/ c^2 and $\Gamma = 0.126 \pm 0.025(\text{stat.})$ GeV/ c^2 . From an analysis with a larger data sample [2], a contribution from $B^+ \rightarrow f_2(1270)K^+$ is also found. However, in this analysis, we do not find a significant signal for $B^0 \rightarrow f_2(1270)K^0$ (see below), so we do not put it in the default model but include this channel when evaluating model uncertainty.

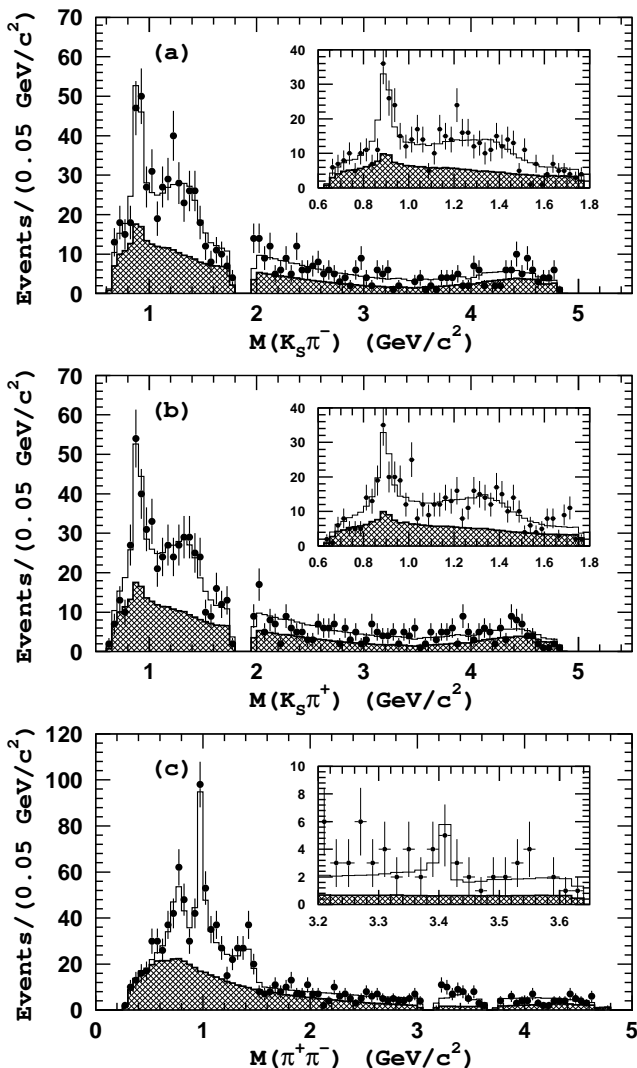


FIG. 4: Results of the fit to $K_S^0 \pi^+ \pi^-$ events in the signal region. Points with error bars are data, the open histograms are the fit result and hatched histograms are the background components. Insets in (a) and (b) show the $K^*(892) - K_0^*(1430)$ mass region in $20 \text{ MeV}/c^2$ bins; inset in (c) shows the χ_{c0} mass region in $25 \text{ MeV}/c^2$ bins. When plotting a two-particle mass projection we require the invariant mass of the other two two-particle combinations to be greater than $1.5 \text{ GeV}/c^2$.

For the non-resonant amplitude \mathcal{A}_{nr} we use an empirical parametrization

$$\mathcal{A}_{\text{nr}}(K^0 \pi^+ \pi^-) = a_1^{\text{nr}} e^{-\alpha s_{13}} e^{i\delta_1^{\text{nr}}} + a_2^{\text{nr}} e^{-\alpha s_{23}} e^{i\delta_2^{\text{nr}}}, \quad (4)$$

where a_i^{nr} , δ_i^{nr} and α are fit parameters. It is worth noting here that a similar parametrization was used not only in the analysis of $B^+ \rightarrow K^+ \pi^+ \pi^-$ [13] but also in $B^+ \rightarrow K^+ K^+ K^-$ decays [13, 19]. Finally, note that, since in this analysis we do not distinguish between B and \bar{B} decays, the signal density function is an incoherent sum

$$S(K_S^0 \pi^\pm \pi^\mp) = |\mathcal{M}(K^0 \pi^+ \pi^-)|^2 + |\mathcal{M}(\bar{K}^0 \pi^- \pi^+)|^2. \quad (5)$$

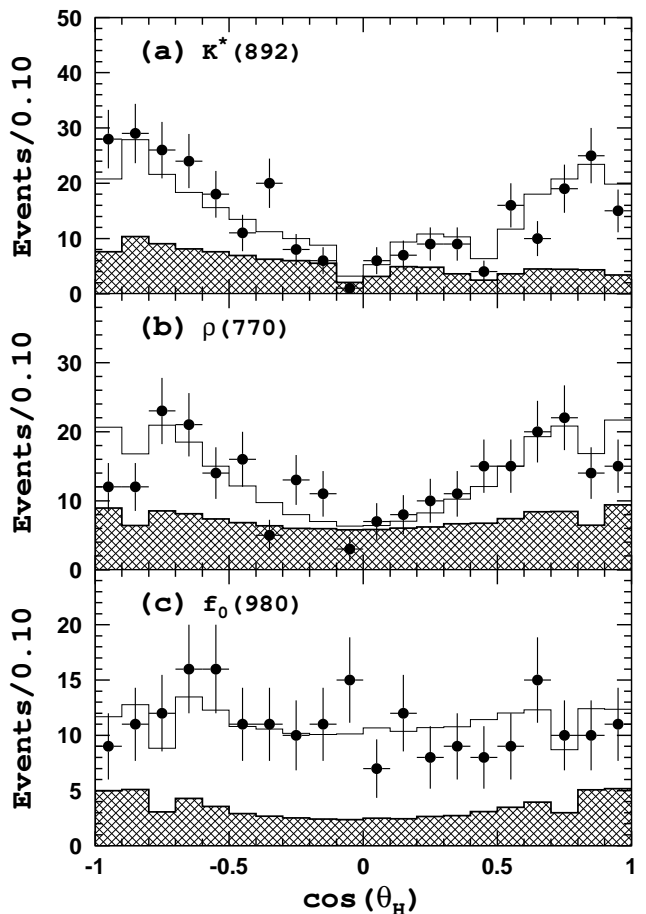


FIG. 5: Helicity angle distributions for (a) $K^*(892)$ ($0.82 \text{ GeV}/c^2 < M(K_S^0 \pi) < 0.97 \text{ GeV}/c^2$); (b) $\rho(770)$ ($0.60 \text{ GeV}/c^2 < M(\pi\pi) < 0.90 \text{ GeV}/c^2$); (c) $f_0(980)$ ($0.90 \text{ GeV}/c^2 < M(\pi\pi) < 1.06 \text{ GeV}/c^2$). Points with error bars are data, the open histogram is the fit result and the hatched histogram is the background component. Note that there are two entries per B candidate in plot (a).

When fitting the data, we choose the $K^*(892)^+ \pi^-$ signal as our reference by fixing its amplitude and phase ($a_{K^*} \equiv 1$ and $\delta_{K^*} \equiv 0$). Two-particle mass projections for the fit and data are compared in Fig. 4. In addition, Fig. 5 shows the helicity angle distributions for several regions. The helicity angle for the $\pi^+ \pi^-$ system is defined as the angle between the π^- flight direction and the B flight direction in the $\pi^+ \pi^-$ rest frame. For the $K_S^0 \pi$ system, the helicity angle is defined with respect to the K_S^0 . All plots in Figs. 4 and 5 demonstrate good agreement between the fit and data. Results of the fit are summarized in Table I, where the relative fraction f_i of a quasi-two-body channel in the three-body signal is calculated as

$$f_i = \frac{\int |a_i \mathcal{A}^i|^2 ds_{13} ds_{23}}{\int |\mathcal{M}|^2 ds_{13} ds_{23}}. \quad (6)$$

While the relative fraction for a particular quasi-two-

TABLE I: Summary of fit results. The first quoted error is statistical, the second is systematic and the third is the model error. R in the two last columns denotes an intermediate resonant state and h stands for a final state hadron: pion or neutral kaon. The $K^0\pi^+\pi^-$ charmless fraction excludes the $B^0 \rightarrow \chi_{c0}K^0$ contribution.

Mode	f_i %	δ_i °	$\mathcal{B}(B \rightarrow Rh) \times \mathcal{B}(R \rightarrow hh) \times 10^6$	$\mathcal{B}(B \rightarrow Rh) \times 10^6$
$K^0\pi^+\pi^-$ charmless	$99.3 \pm 0.4 \pm 0.1$	—	—	$47.5 \pm 2.4 \pm 3.7$
$K^*(892)^+\pi^-$	$11.8 \pm 1.4 \pm 0.5^{+0.9}_{-0.6}$	0 (fixed)	$5.6 \pm 0.7 \pm 0.5^{+0.4}_{-0.3}$	$8.4 \pm 1.1 \pm 0.8^{+0.6}_{-0.4}$
$K_0^*(1430)^+\pi^-$	$64.8 \pm 3.9 \pm 0.5^{+1.6}_{-6.3}$	$45 \pm 9 \pm 2^{+9}_{-13}$	$30.8 \pm 2.4 \pm 2.4^{+0.8}_{-3.0}$	$49.7 \pm 3.8 \pm 6.7^{+1.2}_{-4.8}$
$K^*(1410)^+\pi^-$	—	—	< 3.8	—
$K^*(1680)^+\pi^-$	—	—	< 2.6	—
$K_2^*(1430)^+\pi^-$	—	—	< 2.1	—
$\rho(770)^0K^0$	$12.9 \pm 1.9 \pm 0.3^{+2.1}_{-2.2}$	$-7 \pm 28 \pm 7^{+27}_{-13}$	$6.1 \pm 1.0 \pm 0.5^{+1.0}_{-1.1}$	$6.1 \pm 1.0 \pm 0.5^{+1.0}_{-1.1}$
$f_0(980)K^0$	$16.0 \pm 3.4 \pm 0.8^{+1.0}_{-1.4}$	$36 \pm 34 \pm 5^{+38}_{-21}$	$7.6 \pm 1.7 \pm 0.7^{+0.5}_{-0.7}$	—
$f_X(1300)K^0$	$3.7 \pm 2.2 \pm 0.3^{+0.5}_{-0.5}$	$-135 \pm 25 \pm 2^{+26}_{-31}$	—	—
$f_2(1270)K^0$	—	—	< 1.4	—
Non-resonant	$41.9 \pm 5.1 \pm 0.6^{+1.4}_{-2.5}$	$\delta_1^{\text{nr}} = -22 \pm 8 \pm 1^{+6}_{-6}$ $\delta_2^{\text{nr}} = 175 \pm 30 \pm 4^{+54}_{-30}$	—	$19.9 \pm 2.5 \pm 1.6^{+0.7}_{-1.2}$
$\chi_{c0}K^0$	—	—	< 0.56	< 113

body channel depends only on the corresponding amplitude in the matrix element in Eq. 2, its statistical error depends on the statistical errors of all amplitudes and phases. To determine the statistical errors for quasi-two-body channels, we use a MC pseudo-experiment technique as described in Ref. [13].

We find that a significant fraction of the $B^0 \rightarrow K^0\pi^+\pi^-$ signal is due to a non-resonant-like decay and is dominated by the $K-\pi$ component of the non-resonant amplitude in Eq. (4): $a_2^{\text{nr}}/a_1^{\text{nr}} = 0.20 \pm 0.11(\text{stat.})$. This is in agreement with the analysis of $B^+ \rightarrow K^+\pi^+\pi^-$. The value of the parameter $\alpha = 0.154 \pm 0.033(\text{stat.})$ of the non-resonant amplitude obtained from the fit also agrees with that determined in the analysis of charged B meson decay: $\alpha(K^+\pi^+\pi^-) = 0.195 \pm 0.018(\text{stat.})$ [2].

To determine the reconstruction efficiency for the three-body $B^0 \rightarrow K^0\pi^+\pi^-$ decay, we use MC simulation, where events are distributed over phase space according to the matrix element obtained from the best fit to data. The corresponding reconstruction efficiency is $(6.71 \pm 0.03)\%$ (including the $K^0 \rightarrow \pi^+\pi^-$ branching fraction). Branching fraction results are given in Table I. Since the nature of the $f_X(1300)$ is not well understood, and it might in fact be a mixture of several states (for example, $f_0(1370)$ and $f_0(1500)$), only a relative fraction and phase are given for the $f_X(1300)K^0$ channel. Note that the $B^0 \rightarrow K_S^0\pi^+\pi^-$ signal yield determined from the fit to the ΔE distribution includes some contribution from the $B^0 \rightarrow \chi_{c0}K_S^0$ decay, which is not a charmless decay. To correct for this contribution, we multiply the signal yield by a factor 0.993 (see Table I) when calculating branching fractions.

For the final states where no statistically significant signal is observed, we calculate 90% confidence level upper limits f_{90} for their fractions via

$$0.90 = \frac{\int_0^{f_{90}} G(f, \sigma_f; x) dx}{\int_0^\infty G(f, \sigma_f; x) dx}, \quad (7)$$

where $G(f, \sigma_f; x)$ is a Gaussian function with the measured mean value f for a quasi-two-body signal fraction and its statistical error σ_f . To account for the model uncertainty we determine the relative fractions with various parametrizations of the B decay amplitude (see below) and use the largest value to evaluate the upper limit. To account for the systematic uncertainty, we decrease the reconstruction efficiency by one standard deviation.

To assess how well any given fit represents the data, the Dalitz plot is subdivided into non-equal bins requiring that the number of events in each bin exceeds 25. A goodness-of-fit statistic for the multinomial distribution is then calculated as $\chi^2 = -2 \sum_{i=1}^{N_{\text{bins}}} n_i \ln \left(\frac{p_i}{n_i} \right)$, where n_i is the number of events observed in the i -th bin, and p_i is the number of events predicted from the fit [20]. The distribution of this statistic is bounded by a χ^2 distribution with $(N_{\text{bin}} - 1)$ degrees of freedom, and one with $(N_{\text{bin}} - k - 1)$ degrees of freedom, where k is the number of fit parameters [21]. The χ^2/N_{bins} value for the best fit is 124.3/112 with $k = 16$ fit parameters. This corresponds to a confidence level between 2% and 18%. The χ^2/N_{bins} value of the fit to sideband events is 241.7/197 with $k = 10$ fit parameters.

To estimate the model uncertainty we modify the matrix element Eq. (2) to include an additional quasi-two-body amplitude: either $K^*(1410)^+\pi^-$, $K^*(1680)^+\pi^-$, $K_2^*(1430)^+\pi^-$ or $f_2(1270)K^0$ and repeat the fit to data. For none of these channels is a statistically significant signal found. We also try to fit the data assuming $f_X(1300)$ is a vector (tensor) state. In this case its mass and width are fixed at world average values of $\rho(1450)$ ($f_2(1270)$) [14]. Finally we try several alternative parametrizations of the non-resonant amplitude \mathcal{A}_{nr} to estimate the related uncertainty:

- $a_1^{\text{nr}} e^{-\alpha s_{13}} e^{i\delta_1^{\text{nr}}}$
- $a_1^{\text{nr}} e^{-\alpha s_{13}} e^{i\delta_1^{\text{nr}}} + a_2^{\text{nr}} e^{-\alpha s_{23}} e^{i\delta_2^{\text{nr}}} + a_3^{\text{nr}} e^{-\alpha s_{12}} e^{i\delta_3^{\text{nr}}}$

TABLE II: Contributions to the systematic uncertainty (in percent) for the three-body $B^0 \rightarrow K^0\pi^+\pi^-$ branching fraction.

Source	Error %
Efficiency nonuniformity	2.4
Event shape requirements	2.5
Signal yield extraction	5.4
Charged track reconstruction	2.0
Particle identification	2.0
K_S^0 reconstruction	3.0
$N_{B\bar{B}}$ estimation	1.0
Total	7.8

$$\begin{aligned}
 & \bullet \frac{a_1^{\text{nr}}}{s_{13}^\alpha} e^{i\delta_1^{\text{nr}}} + \frac{a_2^{\text{nr}}}{s_{23}^\alpha} e^{i\delta_2^{\text{nr}}} \\
 & \bullet \frac{\sqrt{s_{13}}}{p_s \cot \delta_B - ip_s} + e^{2i\delta_B} \frac{M_{K_0^*} \Gamma_{K_0^*} \frac{M_{K_0^*}}{p_0}}{M_{K_0^*}^2 - s_{13} - iM_{K_0^*} \Gamma_{K_0^*} \frac{M_{K_0^*}}{p_0} \frac{p_s}{\sqrt{s_{13}}}}; \\
 & \cot \delta_B = \frac{1}{ap_s} + \frac{1}{2}rp_s
 \end{aligned}$$

The latter parametrization, where p_0 (p_s) is the momentum of either daughter particle in the $K_0^*(1430)$ rest frame calculated at the nominal (current) mass value, and a and r are parameters, is suggested by the BaBar Collaboration [22]. It is based on results of the partial wave analysis of elastic K - π scattering by the LASS collaboration [23]. In this parametrization the relative fraction and phase between the $K_0^*(1430)$ amplitude and an underlying broad scalar amplitude (that in the LASS analysis is referred to as an effective range term and in our analysis is described by the independent amplitude \mathcal{A}_{nr}) are fixed from LASS data. However, the use of LASS data is limited to the elastic region (i.e. below the $K\eta$ production threshold), thus in BaBar's analysis the effective range term is truncated slightly above the elastic limit and an additional non-resonant (phase-space) term is introduced to describe an excess of signal events at higher $M(K\pi)$. In our analysis additional degrees of freedom introduced by an independent amplitude \mathcal{A}_{nr} lead to a second solution with a slightly worse likelihood value but with a much smaller $K_0^*(1430)\pi$ signal fraction. MC studies confirm that the presence of the second solution is due to an interplay between the two S -wave components: the $K_0^*(1430)\pi$ and \mathcal{A}_{nr} , and is not related to the limited experimental statistics. A similar ambiguity was found in the analysis of $B^+ \rightarrow K^+\pi^+\pi^-$ and $B^+ \rightarrow K^+K^+K^-$ decays [13, 19]. However, comparison of the phase shift of the total K - π S -wave amplitude (which is a coherent sum of $K_0^*(1430)$ and \mathcal{A}_{nr}) as a function of $M(K\pi)$ with that measured by LASS in the elastic region favors the solution with a large $K_0^*(1430)\pi$ fraction. This is also in agreement with some phenomenological estimates [24].

The dominant sources of systematic error in the determination of the three-body $B^0 \rightarrow K^0\pi^+\pi^-$ branching fractions are listed in Table II. Because of the non-uniformity of the reconstruction efficiency over the Dalitz

plot, the reconstruction efficiency for the three-body $B^0 \rightarrow K^0\pi^+\pi^-$ decay determined from MC is sensitive to the model used to generate signal events. The associated systematic uncertainty is estimated by varying the relative phases and amplitudes of the quasi-two-body states within their errors. The systematic uncertainty due to requirements on event shape variables is estimated from a comparison of their distributions for signal MC events and $B \rightarrow D\pi$ and $B \rightarrow J/\psi K$ events in the data. We estimate the uncertainty in the signal yield extraction from the fit to the ΔE distribution by varying the parameters of the fitting function within their errors. This includes variation of parameters of the signal function, normalization of the $B\bar{B}$ related background and the slope and normalization of the $q\bar{q}$ background function within their errors. The uncertainty from the particle identification efficiency is estimated using pure samples of kaons and pions from $D^0 \rightarrow K^-\pi^+$ decays, where the D^0 flavor is tagged using $D^{*+} \rightarrow D^0\pi^+$. The systematic uncertainty in charged track reconstruction is estimated using partially reconstructed $D^* \rightarrow D\pi$ events and from comparison of the ratio of $\eta \rightarrow \pi^+\pi^-\pi^0$ to $\eta \rightarrow \gamma\gamma$ events in data and MC. For the quasi-two-body channels, additional sources are the uncertainty in parametrization of the distribution of background events over the Dalitz plot that is estimated by varying the parameters of the fitting function Eq. (1) within their errors. Finally, there is an 11% uncertainty in the branching fraction for the $K_0^*(1430) \rightarrow K\pi$ decay [14].

In summary, an amplitude analysis of the three-body charmless $B^0 \rightarrow K^0\pi^+\pi^-$ decay is performed for the first time. The results are summarized in Table I. The analysis reveals the presence of the $K^*(892)^+\pi^-$, $K_0^*(1430)^+\pi^-$, $\rho(770)^0K^0$ and $f_0(980)K^0$ quasi-two-body intermediate channels for which we measure the branching fractions. The $B^0 \rightarrow \rho(770)^0K^0$ branching is measured for the first time. We also find that a significant fraction of the $B^0 \rightarrow K^0\pi^+\pi^-$ signal is due to a non-resonant component; this is consistent with results from the Dalitz analysis of $B^+ \rightarrow K^+\pi^+\pi^-$ decays. We obtain upper limits on branching fractions for several other possible channels; these constraints include the first limits obtained for $K^*(1410)^+\pi^-$, $K^*(1680)^+\pi^-$, $K_2^*(1430)^+\pi^-$ and $f_2(1270)K^0$.

We thank the KEKB group for the excellent operation of the accelerator, the KEK cryogenics group for the efficient operation of the solenoid, and the KEK computer group and the National Institute of Informatics for valuable computing and Super-SINET network support. We acknowledge support from the Ministry of Education, Culture, Sports, Science, and Technology of Japan and the Japan Society for the Promotion of Science; the Australian Research Council and the Australian Department of Education, Science and Training; the National Science Foundation of China and the Knowledge Innovation Program of the Chinese Academy of Sciences under contract No. 10575109 and IHEP-U-503; the Department of Science and Technology of India; the BK21 program of the

Ministry of Education of Korea, the CHEP SRC program and Basic Research program (grant No. R01-2005-000-10089-0) of the Korea Science and Engineering Foundation, and the Pure Basic Research Group program of the Korea Research Foundation; the Polish State Committee

for Scientific Research; the Ministry of Science and Technology of the Russian Federation; the Slovenian Research Agency; the Swiss National Science Foundation; the National Science Council and the Ministry of Education of Taiwan; and the U.S. Department of Energy.

-
- [1] M.Gronau, J.L.Rosner, Phys. Rev. D **72**, 094031 (2005); S.Fajfer, R.J.Oakes, and T.N.Pham, Phys. Lett. B **539**, 67 (2002); N.G.Deshpande, N.Sinha and R.Sinha, Phys. Rev. Lett. **90**, 061802 (2003); M.Gronau, Phys. Rev. Lett. **91**, 139101 (2003); T.Gershon and M.Hazumi, Phys. Lett. B **596**, 163 (2004). M.Gronau, D.Pirjol, A.Soni and J.Zupan, hep-ph/0608243, Submitted to Phys. Rev. D.
- [2] Belle Collaboration, A.Garmash *et al.*, Phys. Rev. Lett. **96**, 251803 (2006).
- [3] Belle Collaboration, K-F.Chen *et al.*, Phys. Rev. D **72**, 012004 (2005).
- [4] BaBar Collaboration, B.Aubert *et al.*, Phys. Rev. D **71**, 091102 (2005).
- [5] Belle Collaboration, K.Sumisawa *et al.*, Phys. Rev. Lett. **95**, 061801 (2005).
- [6] BaBar Collaboration, B.Aubert *et al.*, Phys. Rev. Lett. **97**, 011801 (2005).
- [7] BaBar Collaboration, B.Aubert *et al.*, Phys. Rev. Lett. **94**, 041802 (2005).
- [8] For the most recent update of the results on studies of CP violation in charmless B meson decays see Heavy Flavor Averaging Group web page:
<http://www.slac.stanford.edu/xorg/hfag/index.html>.
- [9] S.Kurokawa and E.Kikutani, Nucl. Instr. and Meth. A **499**, 1 (2003).
- [10] A.Abashian *et al.*, Nucl. Instr. and Meth. A **479**, 117 (2002).
- [11] R.Brun *et al.*, GEANT 3.21, CERN Report DD/EE/84-1, 1984.
- [12] Belle Collaboration, A.Garmash *et al.*, Phys. Rev. D **69**, 012001 (2004).
- [13] Belle Collaboration, A.Garmash *et al.*, Phys. Rev. D **71**, 092003 (2005).
- [14] Particle Data Group, W.-M.Yao *et al.*, J. Phys. G **33**, 1 (2006).
- [15] M.Wirbel, B.Stech, M.Bauer, Zeit. Phys. C **29**, 637 (1985).
- [16] J.Blatt and V.Weisskopf, *Theoretical Nuclear Physics*. New York: John Wiley & Sons (1952).
- [17] S.M.Flatté, Phys. Lett. B **63**, 224 (1976).
- [18] These values of the $f_0(980)$ parameters are consistent with those reported by the BES collaboration:
BES Collaboration, M. Ablikim *et al.*, Phys. Lett. B **607**, 243 (2005).
- [19] BaBar Collaboration, B.Aubert *et al.*, Phys. Rev. D **74**, 032003 (2006).
- [20] S.Barker and R.Cousins, Nucl. Instr. and Meth. **221**, 437 (1984).
- [21] H.Chernoff and E.L.Lehman, Ann. Math. Stat. **25**, 579 (1954).
- [22] BaBar Collaboration, B.Aubert *et al.*, hep-ex/0408073.
- [23] LASS Collaboration, D.Aston *et al.*, Nucl. Phys. B **296**, 493 (1988).
- [24] V.L.Chernyak, Phys. Lett. B **509**, 273 (2001).
- [25] Belle Collaboration, P.Chang *et al.*, Phys. Lett. B **599**, 148 (2004).